Mechanism of the Difference in the Binding Affinity of *E. coli* tRNA^{Gln} to Glutaminyl-tRNA Synthetase Caused by Noninterface Nucleotides in Variable Loop

Satoshi Yamasaki,* Shugo Nakamura,* Tohru Terada,† and Kentaro Shimizu*
*Department of Biotechnology, Graduate School of Agricultural and Life Sciences, and †Agricultural Bioinformatics Research Unit, Graduate School of Agricultural and Life Sciences, The University of Tokyo, Tokyo, Japan

ABSTRACT Aminoacyl-tRNA synthetases (ARSs) distinguish their cognate tRNAs from many other kinds of tRNAs, despite the very similar tertiary structures of tRNAs. Many researchers have supported the view that this recognition is achieved by intermolecular interactions between tRNA and ARS. However, one of the aptamers of *Escherichia coli* glutamine specific tRNA, var-AGGU, has a higher affinity to ARS than the wild-type, although the sequence difference only lies in the variable loop located on the opposite side of the binding interface with ARS. To understand the reason for the difference in affinity, we did molecular dynamics simulations on tRNAs and their complexes with ARS. We calculated the enthalpic and entropic contributions to the binding free energy with the molecular mechanics-Poisson-Boltzmann/surface area method and found that the entropic difference plays an important role in the difference in binding free energies. During the molecular dynamics simulations, dynamic rearrangements of hydrogen bonds occurred in the tertiary core region of the wild-type tRNA, whereas they were not observed in the free var-AGGU simulation. Since the internal mobility was suppressed upon complex formation with ARS, the entropy loss in the wild-type was larger than that of the aptamer. We therefore concluded that the sequence difference in the variable loop caused the difference in the internal mobility of the tertiary core region tRNAs and led to the difference in the affinity to ARS through the entropy term.

INTRODUCTION

The recognition of tRNAs by aminoacyl-tRNA synthetases (ARSs) plays an important role in the central dogma that ensures the accuracy of translation from mRNA to protein. To elucidate the mechanism responsible for precise recognition on a structural basis, the tertiary structures of many kinds of tRNAs, ARSs, and their complexes from various species have been determined. Of these, the system of *Escherichia coli* glutamine-specific tRNA (tRNA^{Gln}) and glutaminyl-tRNA synthetase (GlnRS) is one of those that have been studied most extensively by many researchers (1–4). The tertiary structure of their complex has been solved by x-ray crystallography (PDB ID: 1GTR) (5), and the critical bases of tRNA^{Gln} for recognition by GlnRS, called identity elements, have been determined using biochemical methods. According to Giegé's review (6), G73, U1:A72, G2:C71, G3:C70 (acceptor-stem region), C34, U35, G36, A37, U38 (anticodon region), and G10 (D stem region) are the identity elements of tRNA^{Gln}. All these bases are involved in direct interactions with GlnRS in the tertiary structure.

Intermolecular interactions, especially ones in which identity elements are involved, are thus thought to be the most important in tRNA recognition. However, Bullock et al. (7) reported an exceptional case in which the bases of tRNA^{Gln} far from the binding interface have a remarkable effect on the affinity to GlnRS. They studied the binding of wild-type tRNA^{Gln} and its derivatives, aptamer T1 and aptamer var-AGGU (Fig. 1), to GlnRS using a gel-shift assay and determined their dissociation constants (K_d) (7.1 nM for the wild-type, 0.13 nM for aptamer T1 and 0.27 nM for aptamer var-AGGU). As shown in Fig. 1, the nucleotide sequence for var-AGGU is different from the wild-type only in the variable loop. Var-AGGU has 26 times lower K_d than the wild-type, which corresponds to the difference in the binding free energy of $\sim$8 kJ mol^{-1}. Although aptamer T1 has additional mutations in the T and D loops, its K_d value is only approximately half that of var-AGGU. This suggests that the replacement of the CAUUC sequence in the variable loop of the wild-type tRNA^{Gln} with AGGU is essential for the high affinities of aptamers. Since the variable loop is located on the opposite side of the GlnRS-binding interface in the structure of the wild-type tRNA^{Gln}-GlnRS complex, they determined the crystal structure of the complex with var-AGGU (PDB ID: 1EXD). However, the difference between the complex structures was too small to explain the mechanism responsible for the high affinity from a comparison of the structures. Therefore, they hypothesized that the difference in affinity results from entropic factors.

To address this problem, we did molecular dynamics (MD) simulations on wild-type tRNA, var-AGGU tRNA, and tRNA-GlnRS complexes. We first estimated the enthalpic and entropic contributions to the binding free energy from the MD trajectories. We then conducted principal component analysis (PCA) (8–13) to characterize the difference in entropy. Based on these results, we will discuss the mechanism for the higher affinity of var-AGGU to GlnRS.

Submitted July 21, 2006, and accepted for publication September 15, 2006.
Address reprint requests to S. Nakamura, E-mail: shugo@bi.a.u-tokyo.ac.jp.

0006-3495/07/01/192/09 $2.00
doi: 10.1529/biophysj.106.093351

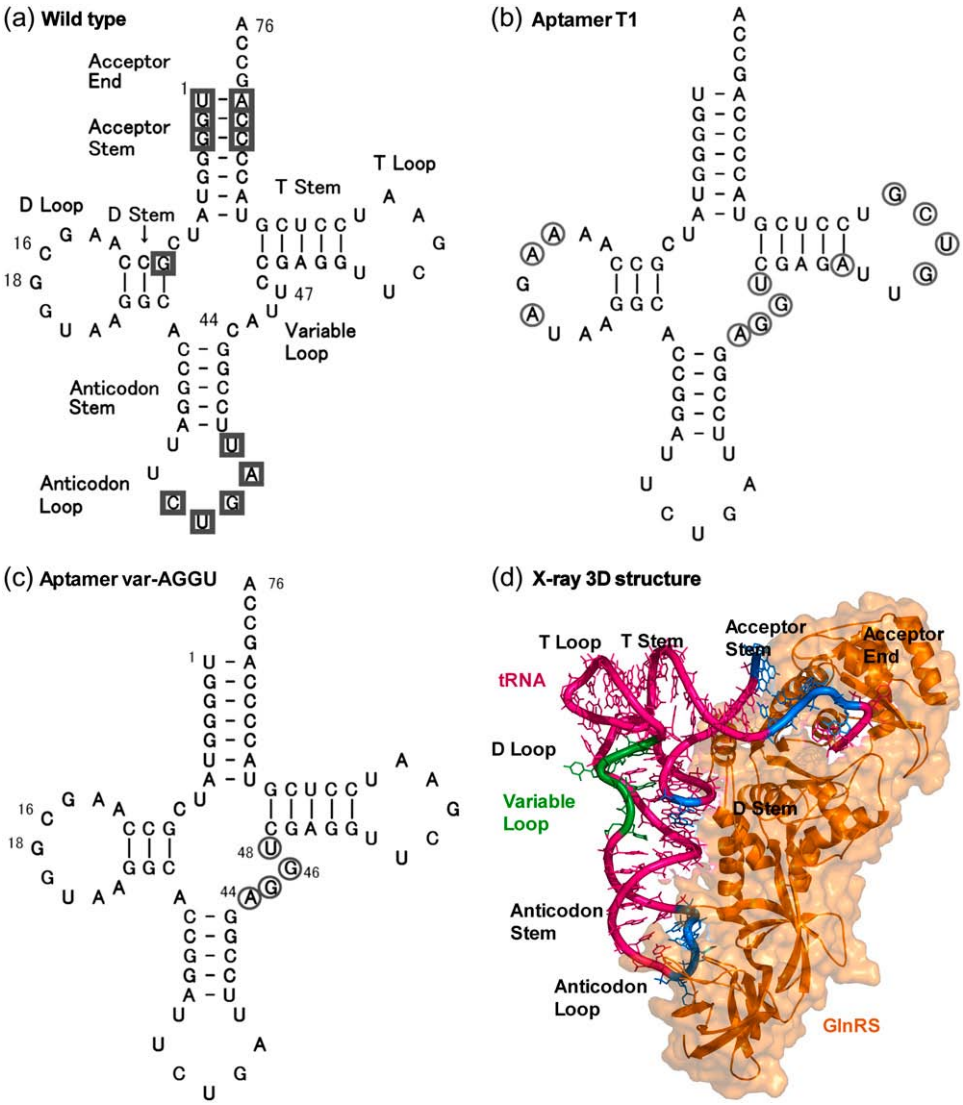

FIGURE 1 Nucleotide sequences of (*a*) wild-type, (*b*) aptamer T1, and (*c*) aptamer var-AGGU in cloverleaf representations. Nucleotides of identity elements are indicated by squares in wild-type sequence. Nucleotides that are different from those of wild-type are indicated by circles in aptamer sequences. (*d*) Crystal structure of complex of wild-type $tRNA^{Gln}$ and GlnRS.

METHODS

MD simulations

In the MD simulations of the tRNA-ARS complexes, the crystal structures obtained from the Protein Data Bank (PDB) (14) (PDB ID: 1GTR (5) for the wild-type tRNA-ARS complex and 1EXD (7) for the var-AGGU-ARS complex) were used as the initial coordinates. Since the structures of the tRNAs in the free forms have not yet been experimentally determined, we modeled these structures as follows. First, the coordinates of the tRNAs were taken from those of the complex structures. The structures of the tRNAs in the complexes with ARS were, however, significantly different from the free $tRNA^{Phe}$ structure (PDB ID: 1EHZ (15)). In these structures, the 3′ end of the acceptor stem makes a hairpin turn and the stacking between the bases of the anticodon loop is disrupted. Therefore, we secondly superimposed the backbone atoms (P, O3′, C3′, C4′, C5′, O5′) of A31–U33 and A37–U39 of the tRNAs onto the corresponding atoms of the free $tRNA^{Phe}$ structure and replaced the coordinates of the anticodon region with those of the $tRNA^{Phe}$. Thirdly, the bases from the $tRNA^{Phe}$ were replaced with those of the tRNAs in question. The coordinates of the end of the acceptor-stem region (G2 and A72–A76) were also modified by the same method. Each structure was immersed in a truncated octahedral box of TIP3P (16) water molecules using the LEaP program of AMBER 7 (17). Neutralizing NH_4^+ ions were added to the system (18,19). The AMBER parm99 force-field parameters (20) were used for the tRNAs, ARS, and counterions. After 2000-step energy minimizations, the systems were gradually heated from 0 to 298 K and equilibrated in 1 ns for the free tRNAs and in 500 ps for the complexes. Production runs were carried out for 6.5 ns. All MD simulations were conducted at constant NPT with the weak-coupling algorithm (21) with a time step of 2 fs. The pressures were kept at 1 bar. The bond lengths involving hydrogen atoms were constrained by using the SHAKE algorithm (22). Electrostatic interactions were calculated by using the particle mesh Ewald method (23–25), and van der Waals interactions were calculated with a cutoff radius of 9.0 Å. The simulations were repeated three times for the free tRNAs, changing the initial velocities.

Calculation of free energies

The free energy can be expressed as the sum of gas-phase enthalpy, solvation free energy, and vibrational entropy. The gas-phase enthalpy and the solvation free energy for each state were calculated with the molecular mechanics-Poisson-Boltzmann/surface area (MM-PB/SA) method (26–28), as average values calculated for snapshot structures recorded during the MD

simulation. The nonpolar contribution to the solvation free energy was estimated by using an empirical relation (29), $\gamma A + b$, where A is the solvation-accessible surface area and γ and b are empirical constants. Here, solvation-accessible surface area was estimated with the MolSurf program (30) and the values of γ and b were 0.0301 and 0.00 kJ mol^{-1}, respectively. The polar contribution was calculated by solving the Poisson-Boltzmann equation numerically with the Delphi program (31).

The vibrational entropy was estimated from the covariance matrix in the Cartesian coordinate system calculated from the MD trajectory (32) as

$$S = 0.5\,k\,\ln\det[\mathbf{1} + (kTe^2/\hbar^2)\boldsymbol{\sigma}], \quad (1)$$

where e is the Euler number, $\hbar = h/2\pi$, and h is Planck's constant. The elements of the covariance matrix, $\boldsymbol{\sigma}$, are given by

$$\sigma_{ij} = \langle x_i - \langle x_i\rangle\rangle\langle x_j - \langle x_j\rangle\rangle, \quad (2)$$

where $x_1,\ldots,x_{3N}$ are the mass-weighted coordinates of the N-particle system and $\langle\ldots\rangle$ denotes the average over the simulation time. The preliminary entropy values were calculated for different simulation periods t (2, 3, 4, 5, and 6 ns for the free tRNAs, and 3, 4, 5, and 6 ns for complexes) and were plotted against $1/t$. The value obtained by extrapolating the plot to infinite simulation times (i.e., $1/t = 0$) was used as the entropy of the system. Due to limitations with computational resources, only the positions of non-hydrogen atoms were considered in the calculations.

Diagonalizing covariance matrix $\boldsymbol{\sigma}$ yielded a set of eigenvectors and eigenvalues corresponding to the modes of the collective motion of the system and the squares of their amplitudes, respectively. This is well known as principal component analysis (PCA). We applied PCA to the ensemble of the backbone atoms of G4–G29, C41–G43, and C49–C69 to analyze the dynamics of the tertiary core regions of tRNAs.

RESULTS AND DISCUSSION

MD simulations

We did 6.5-ns MD simulations on wild-type and var-AGGU tRNAs, and their complexes with GlnRS in an aqueous environment with explicit water. Since the free-form structures of tRNAs have not yet been experimentally determined, we modeled these using complex structures and a free tRNA^{Phe} structure. We therefore repeated the simulations for the free states three times changing the initial velocities. Fig. 2 shows the time evolution for the root mean-square deviations (RMSDs) of the backbone atoms (C_α, N, C for ARSs, and P, O3′, C3′, C4′, C5′, O5′ for tRNAs) from the initial structures during the simulations. The simulations of the complexes revealed small deviations, whereas the values from the simulations of the free tRNAs were large, indicating relaxation from the modeled structures. Since all the systems can be assumed to reach equilibria within 0.5 ns from these plots, we used the trajectories after 0.5 ns in further analyses. To confirm whether the simulation time is sufficiently long or not, we partitioned the 6-ns trajectory from each free tRNA simulation into two 3-ns blocks and compared the conformational distributions between the two blocks. The mean of RMSD values from the average structure calculated within each block ranged from 2.15 to 2.75 Å, whereas the RMSD values between the average structures were 1.10–2.31 Å. This indicates that the conformational distributions of the 3-ns blocks fairly overlap with each other and that the conformation spaces were sufficiently sampled during the 6-ns simulations.

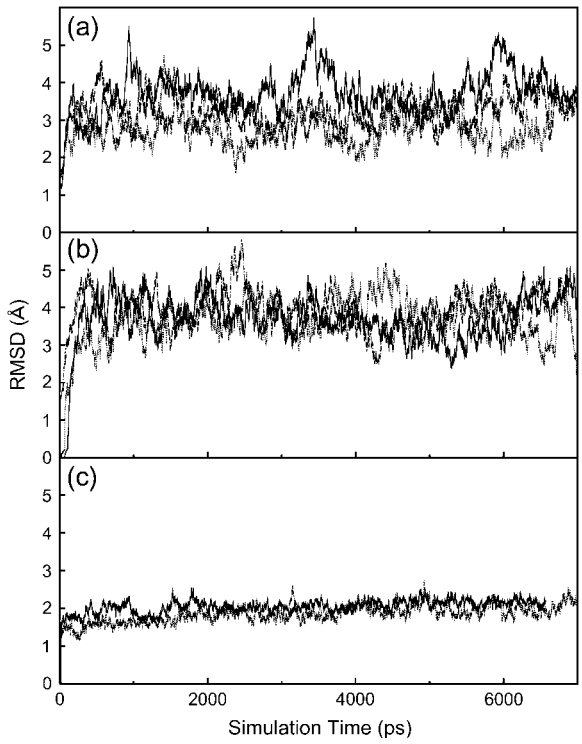

FIGURE 2 Time evolutions of RMSDs calculated for backbone atoms of (*a*) wild-type tRNA in free state and of (*b*) var-AGGU tRNA in free state. Data from first, second, and third runs are plotted with solid, dotted, and dashed lines, respectively. (*c*) Time evolutions of RMSDs for complexes of wild-type (*solid line*) and var-AGGU (*dotted line*) tRNAs with ARS.

Fig. 3 plots RMSD values from average structures calculated for each nucleotide of the tRNAs. In the acceptor-stem (G2–A7 and U66–A76) and anticodon (C28–G42) regions, the RMSD values are larger in the free states than those in the complex states. Since these regions are located at the ends of the L-shaped structure of tRNA, the large deviations are due to the bending motion characteristics of free tRNAs (33). This motion is suppressed in complexes with ARS (34). In the crystal structure of the free yeast tRNA^{phe} (PDB ID: 1EHZ (15)), which we used as a template in the modeling of the free structures, these regions had large temperature factors. Other crystallographic and computational studies (34–37) have also suggested that free tRNAs have larger fluctuations in these regions. Therefore, we think that the large fluctuations observed in the simulations represent the true nature of the free tRNAs. The peaks specific to the simulations for the wild-type derive from the 46th nucleotide, which is not present in var-AGGU. As shown in Fig. 1, the wild-type tRNA has a longer variable loop than var-AGGU. Since the base of this nucleotide (U46) is exposed to the solvent, U46 exhibited large RMSDs in both simulations for the free and complex states.

Fig. 4 shows superpositions of the average structures used in these analyses. The pairwise RMSDs between the wild-type and var-AGGU tRNAs calculated for backbone atoms

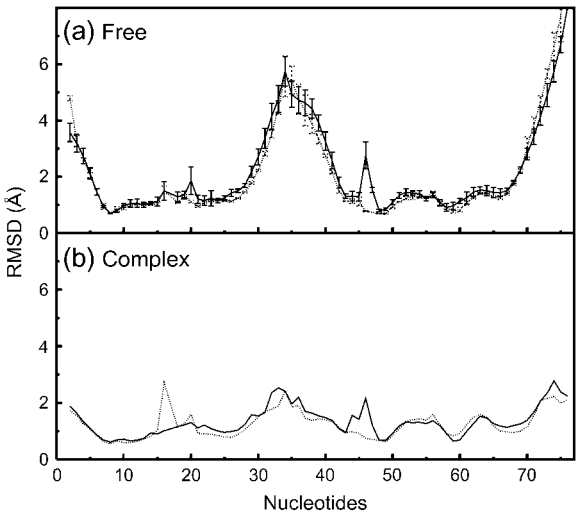

FIGURE 3 (*a*) Nucleotide-averaged RMSD calculated for backbone atoms of wild-type tRNA in free state (*solid line*) and of var-AGGU tRNA in free state (*dotted line*). Data from first, second, and third runs are averaged and plotted with error bars. (*b*) Nucleotide-averaged RMSD calculated for backbone atoms of tRNA in wild-type (*solid line*) and var-AGGU (*dotted line*) complexes.

excluding the variable loops were 4.64 ± 0.84 Å in the free forms and 2.41 ± 0.36 Å in the complex forms. All the intramolecular hydrogen bonds that are important for maintaining the tertiary structure of tRNA (38) were well preserved during the MD simulations in the free state as well as in the complex state.

Analysis of enthalpy and solvation free energy

To clarify what effect the sequence of the variable loop had on the binding free energy, we calculated the enthalpic and entropic contributions to the binding free energy from the MD trajectories using the MM-PB/SA method (26–28). We first examined the contributions the gas-phase enthalpies and the solvation free energies (Table 1) made, because these terms are closely related to intermolecular interactions. The entropic contributions of the solutes will be separately treated in a later section.

The total contribution the sum of the gas-phase enthalpies and the solvation free energies made to the binding free energy difference (i.e., $\Delta\Delta H_{tot} = \Delta H_{tot}$(wild-type) $- \Delta H_{tot}$(var-AGGU)) was -162 ± 12.8 kJ mol^{-1}. Note that the enthalpy and solvation free energy of ARS alone were canceled out in this calculation. The negative sign indicates that the binding of the wild-type tRNA to GlnRS was more preferable than that of the var-AGGU tRNA with respect to these terms. Therefore, the replacement of the nucleotide sequence of the variable loop did not increase the binding affinity enthalpically. Of the electrostatic ($H_{ele} + G_{pol}$), nonpolar ($H_{vdw} + G_{np}$), and internal (H_{int}) energy terms, the electrostatic term made the largest contribution to $\Delta\Delta H$. When the changes due to the replacement of the variable-loop sequence were calculated as the value of the wild-type minus that of var-AGGU, the change in the electrostatic contribution was larger in the complex state [$\Delta(H_{ele}+G_{pol})$(complex) $= -1324$ kJ mol^{-1}] than in the free state [$\Delta(H_{ele}+G_{pol})$(free) $= -1146$ kJ mol^{-1}].

To examine the electrostatic interactions more precisely, we counted the number of intermolecular and intramolecular hydrogen bonds that were formed during >30% of the entire simulation time (Table 2). In the MD simulations, the wild-type had more intermolecular hydrogen bonds than var-AGGU. Although the numbers of hydrogen bonds in which identity elements (6) were involved were almost the same, the numbers of intermolecular hydrogen bonds outside the identity elements were considerably different. This same tendency was observed in the crystal structures. Changes in

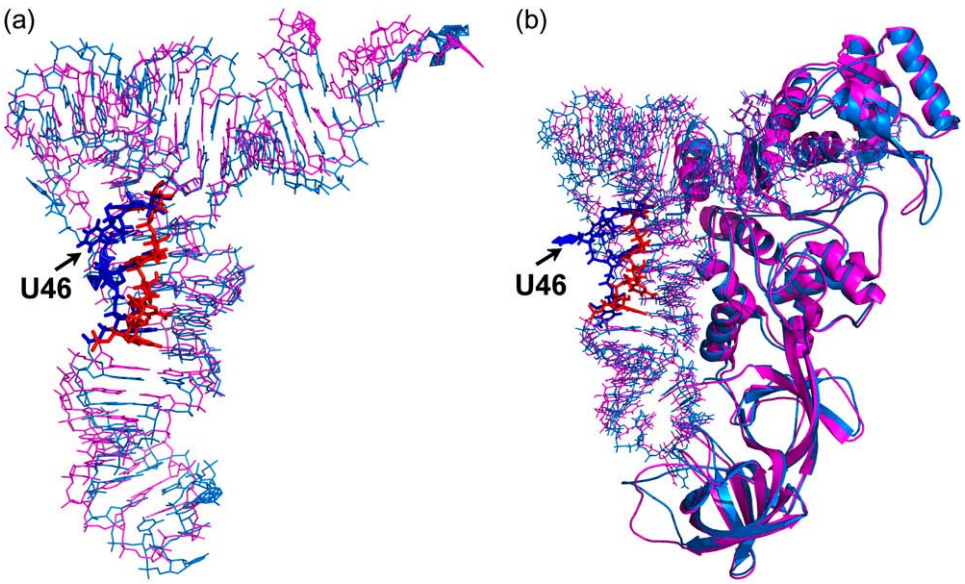

FIGURE 4 (*a*) Superposition of average structure of wild-type tRNA in free state (*light blue*) on that of var-AGGU in free state (*magenta*). (*b*) Superposition of average structure of wild-type tRNA-ARS complex (*light blue*) on that of var-AGGU tRNA-ARS complex (*magenta*). Backbone structures of ARSs are shown with ribbon models. Structures of variable loops of tRNAs are emphasized with blue (wild-type) and red (var-AGGU) thick lines.

TABLE 1 Gas-phase enthalpies and solvation free energies calculated with MM-PB/SA method in kJ mol^{-1} units

	Wild-type		var-AGGU		
	Free	Complex	Free	Complex	$\Delta\Delta H$
H_{ele}	102642.5 ± 383.2	37122.4	96591.7 ± 631.7	34929.9	−3858.2 ± 716.5
H_{vdW}	−3194.6 ± 8.28	−14225.3	−3177.0 ± 29.3	−14188.5	−19.2 ± 30.4
H_{int}	15803.2 ± 3.37	63515.7	15559.5 ± 28.4	63268.6	3.3 ± 28.62
G_{np}	322.7 ± 0.48	1003.6	318.6 ± 0.75	967.9	31.5 ± 0.89
G_{pol}	−184302.2 ± 330.7	−230467.6	−177105.0 ± 599.1	−226951.2	3680.8 ± 684.3
$H_{ele} + G_{pol}$	−81659.7 ± 16.46	−193345.2	−80513.3 ± 39.2	−192021.3	−177.5 ± 42.5
H_{tot}	−68728.3 ± 8.71	−143051.3	−67812.3 ± 9.4	−141973.3	−161.9 ± 12.8

H_{ele}, Electrostatic energy; H_{vdW}, van der Waals energy; H_{int}, internal energy; G_{np}, nonpolar contribution to solvation free energy; G_{pol}, Polar contribution to solvation free energy; $H_{tot} = H_{ele} + H_{vdW} + H_{int} + G_{np} + G_{pol}$; $\Delta\Delta H = [H(\text{wild-type, complex}) - H(\text{wild-type, free})] - [H(\text{var-AGGU, complex}) - H(\text{var-AGGU, free})]$. Standard deviations calculated from values of three runs are shown for free states.

the intramolecular hydrogen bonds due to the replacement of the variable-loop sequence, on the other hand, were almost the same in the free and complex states. Therefore, the sequence replacement in the variable loop had an adverse effect on the binding free energy to ARS through the decrease in the number of intermolecular hydrogen bonds in the region outside the identity elements.

Analysis of entropy

We next examined the entropy term for the binding free energy. Here, we estimated the entropy of each state using the covariance matrix method (32). As shown in Fig. 5, the products of the entropies, S, and the temperature, T (298 K), were well correlated with the inverses of the simulation times ($1/t$) with correlation coefficients >0.99. Therefore, the values of TS were estimated by extrapolating the plots to infinite simulation times (i.e., $1/t = 0$) (Table 3) (32). The difference in the binding entropy change (i.e., $\Delta\Delta TS = \Delta TS(\text{wild-type}) - \Delta TS(\text{var-AGGU})$) was −106.4 ± 109.1 kJ mol^{-1}. Note that the entropy term of ARS is canceled out in the calculation. The negative sign of the average value indicates that the binding of var-AGGU to GlnRS is more preferable than that of the wild-type with respect to entropy. The difference between the entropies of the two complexes was very small (−16 kJ mol^{-1} from Table 3). This may be because the dynamics of the complex state is strongly predominated by GlnRS dynamics (34). Therefore, the difference in the change in binding entropy mainly results from the difference in the free state.

TABLE 2 Number of intramolecular and intermolecular hydrogen bonds observed during simulations in free and complex states and observed in crystal structures

		Wild-type			var-AGGU		
		Free	Complex	Crystal	Free	Complex	Crystal
Intramolecular	tRNA	214	207	122	218	213	139
	GlnRS	–	905	596	–	899	577
Intermolecular	id.	–	13	18	–	11	15
	not id.	–	22	28	–	7	15
	sum	–	35	46	–	18	30

Hydrogen bond is defined as one whose interatomic distance (as measured between heavy atoms) is <3.5 Å. Only bonds that were formed for >30% of whole simulation time have been counted for simulations. Numbers in row of ''id.'' mean those of hydrogen bonds formed with atoms in identity elements of tRNAs.

Internal mobility in tertiary core region of wild-type tRNA

We found that ARS prefers binding wild-type tRNA to binding var-AGGU enthalpically, because it can form more hydrogen bonds with it. However, the wild-type tRNA is unfavorable in terms of entropy, because it loses more entropy on binding to ARS than var-AGGU. From the experiment, we found that var-AGGU binds to ARS more tightly than the wild-type and the difference in the change in binding free energy is ~8 kJ mol^{-1} (7). Although we could not reproduce the experimental values due to difficulties in accurately calculating the difference in free energy from the absolute values of enthalpies and entropies, which included large statistical errors, our results suggest that the difference in entropy in the free states plays an important role in the difference in affinity.

The larger entropy of the wild-type tRNA in the free state implies greater internal mobility or wider conformational distribution in the molecule. To examine the conformational distributions of the tRNAs in free states, we analyzed the principal components of the covariance matrix used in calculating entropy. However, we could not find specific modes that could explain the difference in entropy. This was probably because the large bending motion inherent in the free tRNA obscured relatively small differences in entropy. Therefore, we only examined the conformational distributions of the backbone atoms of G4–G29, C41–G43, and C49–C69 composed of spatial neighbors of the variable loop instead of whole structures, because this region is located in the center of the L-shaped tRNA structure and is not affected by bending motion. Note that this region includes the part of the tertiary core region common to wild-type and var-AGGU tRNAs.

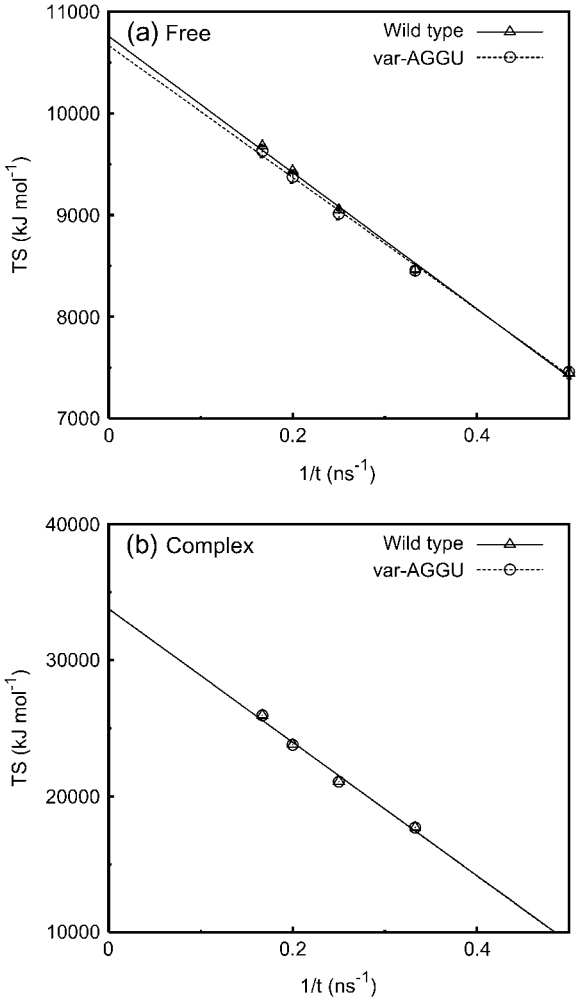

FIGURE 5 Plots of products of entropies S and temperature T of (*a*) free and (*b*) complex states against reciprocal of simulation time t. Data from simulations with wild-type tRNA are plotted with triangles and solid lines and those from var-AGGU are plotted with circles and dashed lines. Average values of three runs are displayed with error bars for free states.

Fig. 6 plots the contribution of each principal mode, converted into entropy, calculated from the conformational distributions for these regions of free tRNAs. The first two principal modes had large differences between wild-type and var-AGGU. Fig. 7 shows projections for the conformational distributions onto planes made by the first and the second principal axes. The distribution for the wild-type is broader

TABLE 3 Product of entropies *S* and temperature *T* calculated by covariance matrix method in kJ mol^{-1} units

	Wild-type free	var-AGGU free	Wild-type Complex	var-AGGU complex
TS	10754.7 ± 67.2	10664.3 ± 124.3	33720.0	33736.0

Standard deviations calculated from values of three runs are shown for free states.

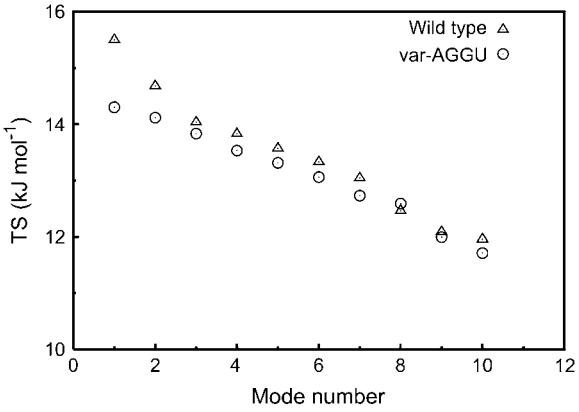

FIGURE 6 Plots of contributions of each principal mode to total entropies calculated from conformational distributions of G4–G29, C41–G43, and C49–C69 of wild-type (*triangles*) and var-AGGU (*circles*) tRNAs in free state.

than that for var-AGGU, and three well-separated conformational clusters can be identified. The distribution for var-AGGU is narrow and is composed of only one conformational cluster. To clarify the cause of multiplicity in the backbone structure for the wild-type in this region, we analyzed the hydrogen bonds bridging this region and the variable loop (Table 4). The hydrogen bonds for which stabilities were different between clusters are shown in Fig. 8. Clusters 1 and

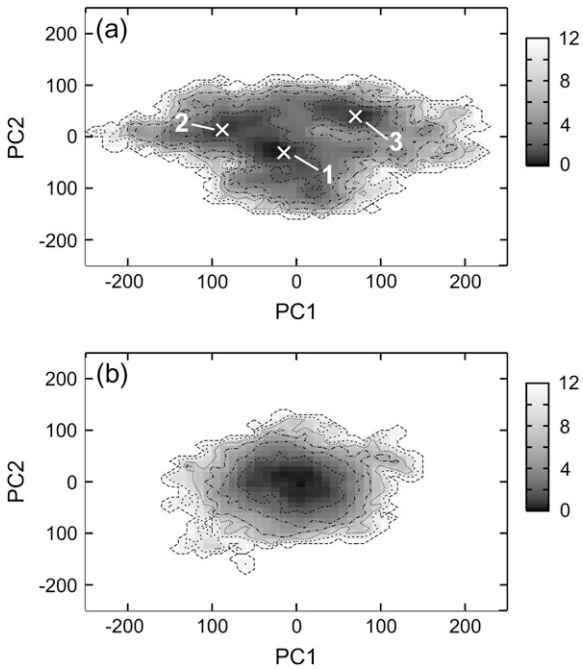

FIGURE 7 Potentials of mean force in kJ mol^{-1} units calculated from conformational distributions on plane of first and second principal axes (in u$^{1/2}$ Å units) of (*a*) wild-type and (*b*) var-AGGU tRNAs in free state. Cluster centers are indicated with crosses together with their identification numbers in plot for wild-type.

TABLE 4 List of hydrogen-bonding atoms pairs in tertiary core region observed during simulation of wild-type tRNA in free state and observed in crystal structure

Pairs		Occupancy % (distance Å)				
		Cluster 1	Cluster 2	Cluster 3	Crystal	
C44O2′	C9N3	19.0 (4.30 ± 0.72)	27.5 (3.87 ± 0.69)	43.6 (3.60 ± 0.71)		
C44O2′	C9O2	35.0 (3.38 ± 0.42)	58.4 (3.16 ± 0.40)	47.4 (3.56 ± 0.55)		(1)
C44O2	C25N4	85.9 (3.27 ± 0.57)	67.3 (3.75 ± 1.15)	92.5 (3.15 ± 0.53)		(2)
C44O2	A26N6	17.6 (3.57 ± 0.53)	25.7 (3.59 ± 0.51)	10.9 (3.73 ± 0.59)	3.09	
C44N3	C25N4	72.2 (3.41 ± 0.54)	42.8 (3.95 ± 1.01)	64.3 (3.44 ± 0.51)		(3)
C44N4	G24N7	77.1 (3.44 ± 0.86)	63.9 (4.32 ± 2.00)	60.5 (3.43 ± 0.71)		(4)
C44N4	G24O1P	88.2 (3.08 ± 0.63)	63.6 (4.07 ± 1.82)	95.1 (2.95 ± 0.37)		(5)
A45N1	A13N6	67.6 (3.58 ± 0.71)	98.9 (3.09 ± 0.17)	34.2 (3.80 ± 0.60)	3.10	(6)
A45N6	A13N1	95.8 (3.10 ± 0.20)	98.1 (3.04 ± 0.16)	92.1 (3.07 ± 0.31)	3.00	
U47O4′	A21N6	89.2 (3.08 ± 0.26)	86.6 (3.14 ± 0.32)	78.9 (3.23 ± 0.47)		
U47N3	A21O1P	99.3 (2.87 ± 0.16)	78.1 (4.22 ± 2.72)	65.4 (3.78 ± 1.41)	3.25	(7)
C48O4′	A21N6	87.9 (3.21 ± 0.29)	73.6 (3.51 ± 0.76)	51.5 (3.54 ± 0.39)		(8)
C48O2	G15N1	71.6 (3.27 ± 0.34)	94.8 (3.15 ± 0.21)	98.9 (2.96 ± 0.17)		
C48N3	G15N2	98.7 (2.96 ± 0.15)	100.0 (2.89 ± 0.09)	99.6 (2.95 ± 0.13)	2.91	
C48N4	A59N7	18.3 (3.71 ± 0.36)	56.5 (3.57 ± 0.42)	12.4 (3.79 ± 0.40)		

Occupancy means fraction of population as percentage that forms hydrogen bonds (interatomic distance is <3.5 Å) in cluster. Average interatomic distances and their standard deviations are shown in parentheses in Å units. Distances between corresponding atom pairs are shown in column of crystal when distances are <3.5 Å. Atom pairs whose average distances are >3.5 Å are underlined (unstable hydrogen bonds). Atom pairs whose hydrogen bonds are stable in one or two clusters and unstable in other clusters are numbered (1–8). These numbers correspond to those in Fig. 8.

3 had a similar pattern for the hydrogen-bond network. Although the non-Watson-Crick hydrogen bond between C44 and A26 observed in the crystal structure was not maintained well during the simulations, C44 formed hydrogen bonds with G24 and C25 in clusters 1 and 3 instead, whereas the base of C44 did not form stable hydrogen bonds in cluster 2. Clusters 1 and 3 were significantly different in the interaction between the N3 of U47 and the phosphate group of A21. In cluster 1, they formed a tight hydrogen bond as in the crystal structure, but the interaction was weak in clusters 2 and 3. In addition, the conformation of U46 in cluster 3, which was exposed to solvent, was quite different from those of clusters 1 and 2, as shown in Fig. 8. Conformational exchange between the structures of clusters 1 and 3 was observed during the first run of the simulations. Although most structures for the second and third runs were included in clusters 2 and 1, respectively, transitions to the structures of the other clusters were observed during the simulations. In this way, the tertiary core region of the wild-type tRNA adopted multiple stable conformations with a dynamic rearrangement of the hydrogen-bond network, whereas rearrangement was not observed during the simulations of free var-AGGU or of the complexes with ARS. It is reasonable to attribute the difference in the internal mobility in this region to the difference in the length and sequence of the variable loop between the wild-type and var-AGGU. Since the internal mobility of the tertiary core region probably has an influence on the mobility of the whole structure, we concluded that the larger entropy of the wild-type tRNA in the free state arises from the greater mobility in the tertiary core region. NMR studies in combination with hydrogen-deuterium exchange experiments are probably useful to verify the internal mobility of the tertiary core region, since they can quantify the strength of the hydrogen bonds and can determine the structure of the hydrogen-bond network in exchange equilibrium.

CONCLUSION

We did molecular dynamics simulations on wild-type tRNA and its variable-loop variant termed var-AGGU, and their complexes with ARS, to clarify why var-AGGU has higher affinity to ARS than the wild-type. We calculated enthalpic and entropic contributions to the binding free energy with the MM-PB/SA method. With respect to enthalpy, sequence replacement in the variable loop has an adverse effect on the binding free energy through a decrease in the number of intermolecular hydrogen bonds. The binding of var-AGGU to GlnRS, on the other hand, is more preferable than that of the wild-type in terms of entropy. Taking the experimental results into account, our results suggest that entropic difference plays an important role in the difference in binding free energies. Since the difference between the entropies of the two complexes was very small, the difference in the change in binding entropy mainly results from the difference in the free state. We examined the conformational distributions of the tertiary core region of the tRNAs and found that dynamic rearrangements of hydrogen bonds occurred in the wild-type tRNA, whereas they were not observed during the simulations of free var-AGGU or the complexes with ARS. We therefore concluded that the sequence difference in the variable loop caused the difference in the internal mobility of the tertiary core region of the tRNAs and this led to the difference in the mobility of the whole structure and in the affinity to ARS through the entropy term.

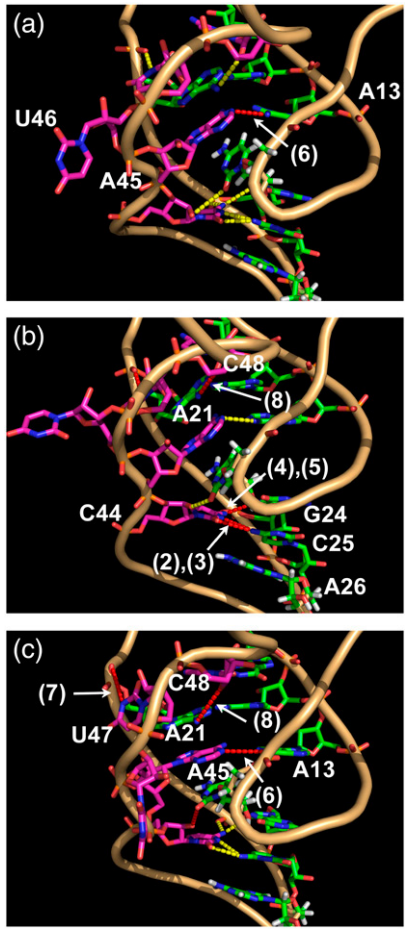

FIGURE 8 Snapshot structures from simulation of wild-type tRNA in free state that are closest to (*a*) first, (*b*) second, and (*c*) third cluster centers identified in Fig. 7. Eight hydrogen-bonds numbered in Table 4 are shown with dotted lines. Stable hydrogen-bonds are in yellow, whereas unstable ones (underlined in Table 4) are in red.

This work was supported in part by Grants-in-Aid for Scientific Research on Priority Areas (grant Nos. 16014204 and 16570132) made available by the Ministry of Education, Culture, Sports, Science and Technology of Japan to K.S.

REFERENCES

1. Rogers, M. J., and D. Söll. 1988. Discrimination between glutaminyl-tRNA synthetase and seryl-tRNA synthetase involves nucleotides in the acceptor helix of tRNA. *Proc. Natl. Acad. Sci. USA.* 85:6627–6631.
2. Jahn, M., M. J. Rogers, and D. Söll. 1991. Anticodon and acceptor stem nucleotides in tRNA(Gln) are major recognition elements for *E. coli* glutaminyl-tRNA synthetase. *Nature.* 352:258–260.
3. Hayase, Y., M. Jahn, M. J. Rogers, L. A. Sylvers, M. Koizumi, H. Inoue, E. Ohtsuka, and D. Söll. 1992. Recognition of bases in *Escherichia coli* tRNA(Gln) by glutaminyl-tRNA synthetase: a complete identity set. *EMBO J.* 11:4159–4165.
4. Ibba, M., K. W. Hong, J. M. Sherman, S. Sever, and D. Söll. 1996. Interactions between tRNA identity nucleotides and their recognition sites in glutaminyl-tRNA synthetase determine the cognate amino acid affinity of the enzyme. *Proc. Natl. Acad. Sci. USA.* 93:6953–6958.
5. Rould, M. A., J. J. Perona, D. Söll, and T. A. Steitz. 1989. Structure of *E. coli* glutaminyl-tRNA synthetase complexed with tRNA(Gln) and ATP at 2.8 Å resolution. *Science.* 246:1135–1142.
6. Giegé, R., M. Sissler, and C. Florentz. 1998. Universal rules and idiosyncratic features in tRNA identity. *Nucleic Acids Res.* 26:5017–5035.
7. Bullock, T. L., L. D. Sherlin, and J. J. Perona. 2000. Tertiary core rearrangements in a tight binding transfer RNA aptamer. *Nat. Struct. Biol.* 7:497–504.
8. Ichiye, T., and M. Karplus. 1991. Collective motions in proteins: a covariance analysis of atomic fluctuations in molecular dynamics and normal mode simulations. *Proteins.* 11:205–217.
9. Kitao, A., F. Hirata, and N. Go. 1991. The effects of solvent on the conformation and the collective motions of protein—normal mode analysis and molecular-dynamics simulations of melittin in water and in vacuum. *Chem. Phys.* 158:447–472.
10. Garcia, A. E. 1992. Large-amplitude nonlinear motion in proteins. *Phys. Rev. Lett.* 68:2696–2699.
11. Hayward, S., A. Kitao, F. Hirata, and N. Go. 1993. Effect of solvent on collective motions in globular protein. *J. Mol. Biol.* 234:1207–1217.
12. Amadei, A., A. B. Linssen, and H. J. C. Berendsen. 1993. Essential dynamics of proteins. *Proteins.* 17:412–425.
13. Becker, O. M. 1997. Geometric versus topological clustering: an insight into conformation mapping. *Proteins.* 27:213–226.
14. Berman, H. M., J. Westbrook, Z. Feng, G. Gilliland, T. N. Bhat, H. Weissig, I. N. Shindyalov, and P. E. Bourne. 2000. The protein data bank. *Nucleic Acids Res.* 28:235–242.
15. Shi, H., and P. B. Moore. 2000. The crystal structure of yeast phenylalanine tRNA at 1.93 Å resolution: a classic structure revisited. *RNA.* 6:1091–1105.
16. Jorgensen, W. L., J. Chandrasekhar, J. D. Madura, R. W. Impey, and M. L. Klein. 1983. Comparison of simple potential functions for simulating liquid water. *J. Chem. Phys.* 79:926–935.
17. Case, D. A., D. A. Pearlman, J. W. Caldwell, T. E. Cheatham III, J. Wang, W. S. Ross, C. Simmerling, T. Darden, K. M. Merz, R. V. Stanton, A. Cheng, J. J. Vincent, et al. 2002. AMBER7. University of California, San Francisco.
18. Singh, U. C., F. K. Brown, P. A. Bash, and P. A. Kollman. 1987. An approach to the application of free-energy perturbation-methods using molecular-dynamics—applications to the transformations of CH_3OH^-, CH_3CH_3, H_3O^+-, NH_4^+, glycine-, alanine, and alanine-phenylalanine in aqueous-solution and to $H_3O^+(H_2O)_3^-$, $NH_4^+(H_2O)_3$ in the gas-phase. *J. Am. Chem. Soc.* 109:1607–1614.
19. Auffinger, P., M. S. Louise, and E. Westhof. 1999. Molecular dynamics simulation of solvated yeast $tRNA^{ASP}$. *Biophys. J.* 76:50–64.
20. Wang, J. M., P. Cieplak, and P. A. Kollman. 2000. How well does a restrained electrostatic potential (RESP) model perform in calculating conformational energies of organic and biological molecules? *J. Comput. Chem.* 21:1049–1074.
21. Berendsen, H. J. C., J. P. M. Postma, W. F. Gunsteren, A. DiNola, and J. R. Haak. 1984. Molecular dynamics with coupling to an external bath. *J. Chem. Phys.* 81:3684–3690.
22. Ryckaert, J. P., G. Ciccotti, and H. J. C. Berendsen. 1977. Numerical-integration of Cartesian equations of motion of a system with constraints—molecular-dynamics of N-alkanes. *J. Comput. Phys.* 23: 327–341.
23. Darden, T., D. York, and L. Pedersen. 1993. Particle mesh Ewald—an $N{\cdot}\mathrm{Log}(N)$ method for Ewald sums in large systems. *J. Chem. Phys.* 98:10089–10092.
24. Essmann, U., L. Perera, M. L. Berkowitz, T. Darden, H. Lee, and L. G. Pedersen. 1995. A smooth particle mesh Ewald method. *J. Chem. Phys.* 103:8577–8593.
25. Toukmaji, A., C. Sagui, J. Board, and T. Darden. 2000. Efficient particle-mesh Ewald based approach to fixed and induced dipolar interactions. *J. Chem. Phys.* 113:10913–10927.

26. Tsui, V., and D. A. Case. 2000. Theory and applications of the generalized Born solvation model in macromolecular simulations. *Biopolymers*. 56:275–291.

27. Wang, J., M. Morin, W. Wang, and P. A. Kollman. 2001. Use of MM-PBSA in reproducing the binding free energies to HIV-1 RT of TIBO derivatives and predicting the binding mode to HIV-1 RT of efavirenz by docking and MM-PBSA. *J. Am. Chem. Soc*. 123: 5221–5230.

28. Tsui, V., and D. A. Case. 2001. Calculations of the absolute free energies of binding between RNA and metal ions using molecular dynamics simulations and continuum electrostatics. *J. Phys. Chem. B*. 105:11314–11325.

29. Sitkoff, D., K. A. Sharp, and B. Honig. 1994. Accurate calculation of hydration free energies using macroscopic solvent model. *J. Phys. Chem*. 98:1978–1988.

30. Connolly, M. L. 1993. Analytical molecular-surface calculation. *J. Appl. Crystal*. 16:548–558.

31. Honig, B., and A. Nicholls. 1995. Classical electrostatics in biology and chemistry. *Science*. 268:1144–1149.

32. Schlitter, J. 1993. Estimation of absolute and relative entropies of macromolecules using the covariance-matrix. *Chem. Phys. Lett*. 215: 617–621.

33. Nakamura, S., and J. Doi. 1994. Dynamics of transfer RNAs analyzed by normal mode calculation. *Nucleic Acids Res*. 22:514–521.

34. Nakamura, S., M. Ikeguchi, and K. Shimizu. 2003. Dynamical analysis of tRNA(Gln)-GlnRS complex using normal mode calculation. *Chem. Phys. Lett*. 372:423–431.

35. Bahar, I., and R. L. Jernigan. 1998. Vibrational dynamics of transfer RNAs: comparison of the free and synthetase-bound forms. *J. Mol. Biol*. 281:871–884.

36. Westhof, E., and M. Sundaralingam. 1986. Restrained refinement of the monoclinic form of yeast phenylalanine transfer RNA. Temperature factors and dynamics, coordinated waters, and base-pair propeller twist angles. *Biochemistry*. 25:4868–4878.

37. Wang, Y., and R. L. Jernigan. 2005. Comparison of tRNA motions in the free and ribosomal bound structures. *Biophys. J*. 89:3399–3409.

38. Oliva, R., L. Cavallo, and A. Tramontano. 2006. Accurate energies of hydrogen bonded nucleic acid base pairs and triplets in tRNA tertiary interactions. *Nucleic Acids Res*. 34:865–879.